Processing the Non-parallel Bistatic SAR Data by Using Chirp-z Transform

Jinhe Ran[1,a], Yang Shen[1] and Xiuhe Li[1]

[1] National University of Defense Technology, Hefei, Anhui, China

Abstract. A new analytical imaging algorithm based on Chirp-z transform (CZT) for focusing non-parallel bistatic SAR data is proposed. The reference function multiplication (RFM) is firstly performed to finish the bulk focusing. Then the phase terms of spectrum are decomposed into range phase term and azimuth phase term, and their space-variances are eliminated by CZT independently to finish the differential focusing. The algorithm can be applied to wide scene imaging, and its effectiveness is verified by simulations.

1 Introduction

Parallel translational invariant SAR preserves the advantages of bistatic SAR. Its echo data is azimuth-variant, which facilitates formulating the imaging algorithms [1-2]. However, it is difficult for parallel translational invariant SAR to keep parallel in practical imaging, therefore, the transmitter and receiver fly with non-parallel tracks has more advantages.

Since the echo data of non-parallel bistatic SAR is azimuth-variant, range and azimuth space variances of echo data must be eliminated to get focusing result. The time-domain algorithm [2] can well focus the bistatic SAR in arbitrary flight tracks, but it is quite time consuming. The processing efficiency can be highly improved in the frequency domain [3], and many frequency domain imaging algorithms to focus azimuth-variant bistatic SAR have been reported. In [4-6], a modified NLCSA is proposed to focus general case bistatic SAR. In [7-8], 2-D ISFT, 2-D stolt interpolation are respectively used to eliminate the 2-D space variances of azimuth-variant bistatic SAR echo data.

In this paper, we present a new analytical frequency domain imaging algorithm based on the Chirp-z transform (CZT) for focusing non-parallel bistatic SAR data. The reference function multiplication (RFM) is firstly performed to finish the bulk focusing, then the phase terms of GLBF are decomposed into two independent phase terms as range phase terms and azimuth phase terms. Space-variances of echo signal in range and azimuth are eliminated by CZT independently. Simulations validate the effectiveness of the proposed algorithm.

2 Signal Model

The geometry of non-parallel bistatic SAR is presented in Fig.1. The transmitter and receiver fly on nonparallel track with same velocity. Squint angles of the transmitter and the receiver are denoted by θ_{T0} and θ_{R0} respectively. Position of arbitrary point target (PT) in the imaging scene is denoted by $\boldsymbol{P}_0(R_{R0}, t_{R0})$, where t_{R0} is the azimuth time when the PT $\boldsymbol{P}_0$ is observed perpendicularly from the receiver track, and R_{R0} is the corresponding closest slant range. Similarly, we can define the parameters as t_{T0} and R_{T0} in reference of the transmitter track. The slant range of PT $\boldsymbol{P}_0$ can be defined as

$$R_B(t)=\sqrt{R_{R0}^2+v^2(t-t_{R0})^2}+\sqrt{a_2^2R_{R0}^2+v^2(t-a_0-t_{R0})^2} \tag{1}$$

In (1), t is the azimuth time, $a_0=t_{T0}-t_{R0}$ is the azimuth time difference, and $a_2=R_{T0}/R_{R0}$ is the ratio of closest slant range[1].

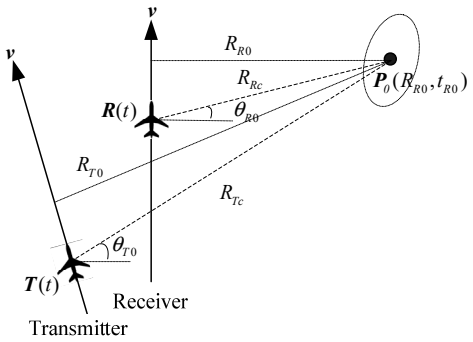

Figure 1. Geometry of non-parallel bistatic SAR

We assume a linear FM (LFM) pulse $s(\tau)=rect(\tau/T_p)\exp\{\mathrm{j}2\pi f_c\tau+\mathrm{j}\pi k_r\tau^2\}$ is transmitted by the transmitter, where k_r is the chirp rate, f_c is the carrier frequency and $rect(\tau/T_p)$ is the rectangle function. The demodulated and normalized echoes from PT $\boldsymbol{P}_0$ can be formulated as

[a] Corresponding author: jinhe_ran@163.com

$$ss(\tau,t;R_{R0},t_{R0})=\exp\{\mathrm{j}\pi k_r(\tau-R_B(t)/c)^2\}\cdot\exp\{-\mathrm{j}2\pi R_B(t)/\lambda\} \tag{2}$$

where τ is the range time, c is the light speed and λ is the wavelength of the transmitted signal.

Performing 2-D Fourier transformation (FT) to (2) and applying the PSP to solve the integral in the derivation, we get the 2-D spectrum of echo signal

$$\begin{aligned}SS_{ra}(f_\tau,f_t;R_{R0},t_{R0}) =&\exp\{-j2\pi(f_t t_{R0}+f_{tT}a_0)\}\\ &\cdot\exp\{-j2\pi R_{R0}[F_R(f_\tau,f_t)+a_2F_T(f_\tau,f_t)]/c\}\\ &\cdot\exp\{-j\pi f_\tau^2/k_r\}\end{aligned} \tag{3}$$

(3) is the signal spectrum in reference of receiver track, which is also named as GLBF[1]. $F_R(f_\tau,f_t)$ and $F_T(f_\tau,f_t)$ are given as

$$\begin{cases}F_R(f_\tau,f_t)=\sqrt{(f_c+f_\tau)^2-(cf_{tR}/v)^2}\\ F_T(f_\tau,f_t)=\sqrt{(f_c+f_\tau)^2-(cf_{tT}/v)^2}\end{cases} \tag{4}$$

In (3) and (4), f_τ and f_t denote the range and Doppler frequency respectively, f_{tR} and f_{tT} denote the instantaneous Doppler frequency of the receiver and transmitter, and given by

$$\begin{cases}f_{tR}=k_R(f_t-f_{dcR}-f_{dcT})+f_{dcR}\\ f_{tT}=k_T(f_t-f_{dcR}-f_{dcT})+f_{dcT}\end{cases} \tag{5}$$

where f_{dcR} and f_{dcT} are the Doppler centroid; k_T and k_R denote the contributions of the transmitter and the receiver to the azimuth chirp rate [8].

$$\begin{cases}f_{dcR}=v\sin\theta_{R0}(f_\tau+f_c)/c\\ f_{dcT}=v\sin\theta_{T0}(f_\tau+f_c)/c\end{cases} \tag{6}$$

3 Formulation of Imaging Algorithm

Data blocking is always performed to decrease the space-variance of echo data in wide scene imaging [4]. Therefore, the first step of algorithm is to block the echo data along the range, and then the conjugate function of the center point target (PT) $\boldsymbol{P}_m(R_{Rm},t_{Rm})$ in the data block is used as reference function to compensate the echo data, which is denoted by

$$\begin{aligned}H_1(f_\tau,f_t;R_{Rm},t_{Rm})=&\exp\{j2\pi(f_{tR}t_{Rm}+f_{tT}t_{Tm})\}\\ &\cdot\exp\{j2\pi[F_R(f_\tau,f_t)R_{Rm}/c+F_T(f_\tau,f_t)R_{Tm}/c]\}\\ &\cdot\exp\{j\pi f_\tau^2/k_r\}\end{aligned} \tag{7}$$

After the reference function multiplication (RFM), the center PT $\boldsymbol{P}_m$ is well focused, but the range and azimuth space variation of echo must be eliminated to get the final imaging result.

Multiplying (3) with (7) giving the following result

$$\begin{aligned}SS_{ra}(f_\tau,f_t;R_{R0},t_{R0})=&\exp\{-j2\pi(f_{tR}\Delta t_R+f_{tT}\Delta t_T)\}\\ &\cdot\exp\{-j2\pi[F_R(f_\tau,f_t)\Delta R_R+F_T(f_\tau,f_t)\Delta R_T]/c\}\end{aligned} \tag{8}$$

With the bistatic geometry, PT position offsets along the transmitter track can be expressed in terms of PT position offsets along the receiver track, and we get

$$\begin{cases}\Delta R_T=A_1\Delta t_R+A_2\Delta R_R\\ \Delta t_T=B_1\Delta t_R+B_2\Delta R_R\end{cases} \tag{9}$$

where

$$\begin{cases}A_1=v\sin\alpha_B\sin\mu_T\\ A_2=\cos\alpha_B\sin\mu_T/\sin\mu_R\\ B_1=\cos\alpha_B\\ B_2=-\sin\alpha_B/(v\sin\mu_R)\end{cases} \tag{10}$$

where μ_T and μ_R are the incident angles when the beam of transmitter and receiver perpendicularly illuminates PT $\boldsymbol{P}_m$ .The bistatic geometry can be transformed to the receiver-referenced geometry with (9). Substituting (9) into (8) and further arranging the results yields

$$\begin{aligned}SS_{ra}^{'}(f_\tau,f_t;R_{R0},t_{R0})=&\exp\left\{-2\pi\left[f_{tR}+B_1f_{tT}+\frac{A_1}{c}F_T(f_\tau,f_t)\right]\Delta t_R\right\}\\ &\cdot\exp\left\{-2\pi\left[B_2f_{tT}+\frac{1}{c}F_R(f_\tau,f_t)+\frac{A_2}{c}F_T(f_\tau,f_t)\right]\Delta R_R\right\}\end{aligned} \tag{11}$$

From (11), we can find that the phase terms are decomposed into two independent phase terms. The first phase term denotes the azimuth phase term which is determined by the azimuth time, while the second phase term represents the range phase term which is determined by the closest slant range. Therefore, space-variances of echo signal can be handled in range and azimuth independently.

We remark the range phase term in (11) as $\Delta\varphi_R(f_\tau,f_t;\Delta R_R)$, and further expand it in the second-order Taylor series in terms of f_τ, giving the following results

$$\Delta\varphi_R(f_\tau,f_t;\Delta R_R)\approx\xi_R(f_t,\Delta R_R)+2\pi\frac{2\Delta R_R}{c}\gamma_R(f_t)f_\tau \tag{12}$$

where

$$\begin{aligned}\xi_R(f_t,\Delta R_R)=-2\pi\Bigg\{&B_2D_T^{'}+\frac{1}{\lambda}\sqrt{1-\lambda^2D_R^{'2}/v^2}\\ &+\frac{A_2}{\lambda}\sqrt{1-\lambda^2D_T^{'2}/v^2}\Bigg\}\Delta R_R\end{aligned} \tag{13}$$

$$\gamma_R(f_t)=-\left\{\frac{cB_2D_T}{2}+\frac{1-\lambda cD_R^{'}D_R/v^2}{2\sqrt{1-\lambda^2D_R^{'2}/v^2}}+\frac{A_2-\lambda A_2cD_T^{'}D_T/v^2}{2\sqrt{1-\lambda^2D_T^{'2}/v^2}}\right\} \tag{14}$$

$$\begin{cases}D_{T,R}^{'}=k_{T,R}f_t+f_cD_{T,R}\\ D_{T,R}=-k_{T,R}v\sin\theta_{R0,T0}/c+k_{R,T}v\sin\theta_{T0,R0}/c\end{cases} \tag{15}$$

In (12), $\xi_R(f_t,\Delta R_R)$ denotes the differential phase modulation of PT $\boldsymbol{P}_0$ with respect to PT $\boldsymbol{P}_m$ in range-Doppler domain. Since it is range-dependent, it has to be removed by phase multiplication in range-Doppler domain. $\gamma_R(f_t)$ is involved in the first-order range frequency and also named as the range scaling factor [9]. It describes the Doppler-dependent RCM with respect to the reference closet range in range-Doppler domain.

We use CZT [10] to correct the scaling factor, and the correction parameters are given by

$$\begin{cases} A(f_t) = \exp\left\{-j\pi\left(1-\dfrac{\gamma(f_t)}{\gamma_{\max}}\right)\right\} \\ W(f_t) = \exp\left\{-j\dfrac{\gamma(f_t)}{\gamma_{\max}}\cdot\dfrac{2\pi}{N_R}\right\} \end{cases} \tag{16}$$

where $\gamma_{\max} = \max[\gamma(f_t)]$, and N_R is the sampling number of the signal in range.

After correcting the range scaling factor, the differential phase modulation must be compensated to eliminate the range space variance of echo, and the compensation function is formulated as

$$H_2(f_t, \Delta R_R) = \exp\left\{-j\xi_R(f_t, \Delta R_R)\cdot\frac{\gamma_{R,\max}}{\gamma_R(f_t=0)}\right\} \tag{17}$$

We remark the azimuth phase term in (11) as $\Delta\varphi_A(f_\tau, f_t; \Delta t_R)$, and further expand it in the second-order Taylor series in terms of f_t, giving the following results

$$\Delta\varphi_A(f_\tau, f_t; \Delta t_R) \approx \xi_A(f_\tau, \Delta t_R) + 2\pi\frac{\Delta t_R}{2}\gamma_A(f_\tau)f_t \tag{18}$$

where

$$\xi_A(f_\tau, \Delta t_R) = -2\pi\left\{E_R + B_1E_T + \frac{A_1}{c}\sqrt{(f_c+f_\tau)^2 - (\frac{cE_T}{v})^2}\right\}\Delta t_R \tag{19}$$

$$\gamma_A(f_\tau) = -\left\{2k_R + 2B_1k_T - \frac{2A_1c^2}{cv^2}\frac{E_Tk_T}{\sqrt{(f_c+f_\tau)^2 - (cE_T/v)^2}}\right\} \tag{20}$$

$$E_{T,R} = k_{R,T}f_{dcT,dcR} - k_{T,R}f_{dcR,dcT} \tag{21}$$

In (18), $\xi_A(f_\tau, \Delta t_R)$ determines the azimuth position of PT $\boldsymbol{P}_m$ that can be compensated by phase multiplication in 2-D frequency domain. $\gamma_A(f_\tau)$ is involved in the linear term of azimuth frequency and also named as the azimuth scaling factor, and it describes the range frequency-dependent RCM of PT $\boldsymbol{P}_0$ with respect to PT $\boldsymbol{P}_m$.

We use CZT [10] to correct the azimuth scaling factor, and the correction parameters are given by

$$\begin{cases} A_A(f_\tau) = \exp\left\{-j\pi\left(1-\dfrac{\gamma_A(f_\tau)}{\gamma_{A,\max}}\right)\right\} \\ W_A(f_\tau) = \exp\left\{-j\dfrac{\gamma_A(f_\tau)}{\gamma_{A,\max}}\cdot\dfrac{2\pi}{N_A}\right\} \end{cases} \tag{22}$$

After correcting the azimuth scaling factor, the differential phase modulation must be compensated to eliminate the azimuth space variance of echo, and the compensation function is formulated as

$$H_3(f_\tau, \Delta t_R) = \exp\{-j\xi_A(f_\tau, \Delta t_R)\} \tag{23}$$

The flowchart of the imaging algorithm is shown in Fig. 2. The first step of algorithm is to block the echo data in range and azimuth with the blocking rules in [4]. Then the reference function multiplication (RFM) is performed in 2-D frequency, and the 2-D space variance of echo is eliminated by 2-D CZT.

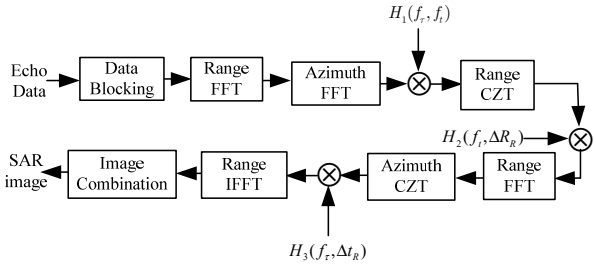

Figure 2. Flow chart of imaging algorithm

4 Simulations

To prove the effectiveness of proposed imaging algorithm, simulations using the bistatic SAR parameters shown in Table 1 are carried out. The imaging scene is set by an array of 9 PTs whose position intervals are all 150m in ground range and azimuth.

Table 1. Simulation parameters

Parameters	**Transmitter**	**Receiver**
Height	6km	8km
Slant range to PT	16.2km	13km
Squint angle	6.5°	3.4°
Velocity of platform	100m/s	100m/s
Length of baseline	7km	
Carrier frequency	10GHz	
Pulse width	10us	
Pulse bandwidth	75 MHz	

Focusing result of the whole imaging scene is presented in Fig. 3, and it shows that we obtain ideal focusing result of whole imaging scene. Fig.4 shows the close look at focusing result of PT A, PT B, PT C, and PT D, which are extracted from the focusing result of whole scene. From Fig.4, we can find that all PTs on the margin of imaging scene are well focused both in range and azimuth. To further evaluate the focusing performance of algorithm, peak sidelobe ratio (PSLR) and integrated sidelobe ratio (ISLR) in range and azimuth (with no weighting function) of four PTs in Fig.3 are calculated, and the results are listed in Table 2. From the measured parameters and focusing result, we can find that all performance parameters of four PTs approximate to the theoretical values, which validates the proposed imaging algorithm to focus non-parallel Bistatic SAR.

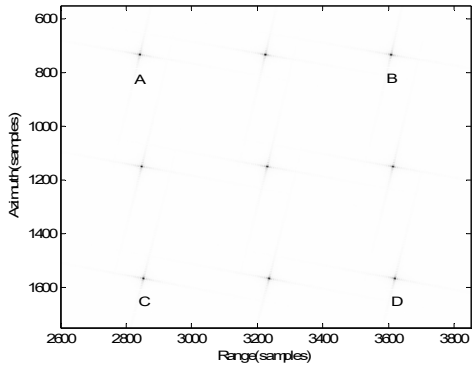

Figure 3. Focusing result of whole imaging scene

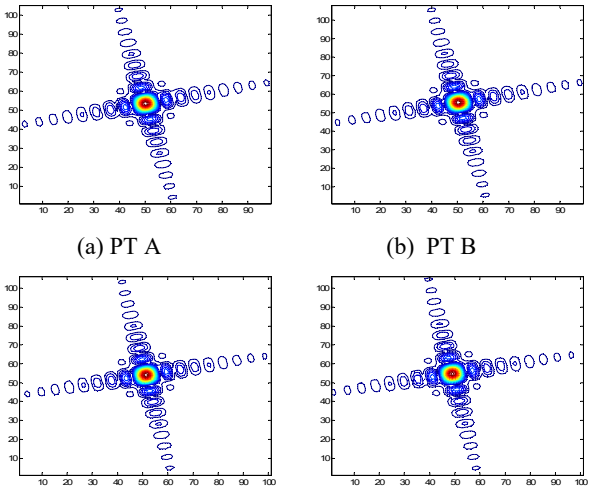

(a) PT A (b) PT B

(c) PT C (d) PT D

Figure 4. Close look at focusing result of four PTs

Table 2. Focusing performance of four PTs

PT	Range		Azimuth	
	PSLR (dB)	ISLR (dB)	PSLR (dB)	ISLR (dB)
PT A	-13.21	-10.11	-13.14	-10.22
PT B	-13.35	-10.08	-13.27	-10.13
PT C	-13.29	-10.21	-13.11	-10.07
PT D	-13.31	-10.15	-13.17	-10.17

5 Conclusions

In this paper, an analytical frequency domain imaging algorithm based on CZT for non-parallel bistatic SAR is introduced. The bistatic geometry is transformed to the receiver-referenced geometry, then the range and azimuth scaling factors are derived and further corrected by CZT independently. The imaging algorithm is high efficient because the whole procedure only contains FFT operations and phase multiplications, and its effectiveness is validated by simulations.

References

1. R. Wang , Y. K. Deng, O. Loffeld, et al. Processing the azimuth–variant bistatic SAR data by using monostatic imaging algorithm based on two-dimensional principle of stationary phase. IEEE Trans. on Geoscience and Remote Sensing, **49**, 7(2011)
2. T. Vu Viet, I. P. Mats. Fast backprojection algorithm based on subapertures and local polar coordinates for general bistatic airborne SAR systems. IEEE Trans. on Geoscience and Remote Sensing, **54**, 5 (2016)
3. R. Wang, O. Loffeld, H. Nies, et al. Frequency-domain bistatic SAR Processing for spaceborne/airborne configuration. IEEE Trans. on Aerospace and Electronic Systems, 2010, **46**,3 (2010)
4. F. H. Wong, I. G. Cumming, Y. L. Neo. Focusing bistatic SAR data using the nonlinear chirp scaling algorithm. IEEE Trans. on Geoscience and Remote Sensing, **46**, 9(2008)
5. H. Zhong, S. Zhang, J. Hu, M. H. Song. Focusing nonparallel-track bistatic SAR data using extended nonlinear chirp scaling algorithm based on a quadratic ellipse model. IEEE Geoscience and Remote Sensing Letters, **14**,12 (2017)
6. D. Li, W. Wang, H. Q. Liu, H. L. Cao, H. Lin. Focusing Highly Azimuth Variant Bistatic SAR. IEEE Transactions on Aerospace and Electronic Systems, **52**, 6 (2016)
7. K. Natroshvili, O. Loffeld, H. Nies, et al. Focusing of general bistatic SAR configuration data with 2-D inverse scaled FFT. IEEE Trans. on Geosciences and Remote Sensing, **44**,10(2006)
8. R. Wang, O. Loffeld, H. Nies, et al. Focusing spaceborne/airborne hybrid bistatic SAR data using wavenumber-domain algorithm. IEEE Trans. on Geoscience and Remote Sensing, **47**,7(2009)
9. I. G. Cumming, F. H. Wong. *Digital processing of synthetic aperture radar data: algorithms and implemnentations.* Norwood: Artech House, 2005
10. R. Lanari. A new method for the compensation of the SAR range cell migration based on the chirp z-transform. IEEE Tran. on. Geoscience and Remote Sensing, **33**,5(1995)